In situ Calibration of Neutron Activation System on the Large Helical Device

N. Pu[1], T. Nishitani[2], M. Isobe[1,2], K. Ogawa[1,2], H. Kawase[1], T. Tanaka[3], S. Y. Li[3],

S. Yoshihashi[3], and A. Uritani[3]

[1]SOKENDAI (The Graduate University for Advanced Studies),

322-6 Oroshi-cho, Toki 509-5292, Japan

[2]National Institute for Fusion Science, National Institutes of Natural Sciences,

322-6 Oroshi-cho, Toki 509-5292, Japan

[3]Nagoya University, Furo-cho, Nagoya, 464-8603, Japan

Abstract

In situ calibration of the neutron activation system on the Large Helical Device (LHD) was performed by using an intense ^{252}Cf neutron source. To simulate a ring-shaped neutron source, we installed a railway inside the LHD vacuum vessel and made a train loaded with the ^{252}Cf source running along a typical magnetic axis position. Three activation capsules loaded with 30 pieces of indium foil-stacked with total mass of approximately 18 g were prepared. Each capsule was irradiated over 15 hours while the train was circulating. The activation response coefficient $(9.40\pm1.21) \times 10^{-8}$ of ^{115}In(n, n')^{115m}In reaction obtained from the experiment is in good agreement with results by three-dimensional neutron transport calculations using the MCNP 6 code. The activation response coefficients for 2.45 MeV birth neutron and secondary 14.1 MeV neutron from deuterium plasma were evaluated from the activation response coefficient obtained at this calibration experiment.

I. INTRODUCTION

The Large Helical Device (LHD) is a large superconducting heliotron device in Japan, having a major radius of 3.9 m and averaged plasma minor radius of ~0.6 m.[1] In LHD, deuterium plasma operation was conducted from March 2017 to explore further high-performance deuterium plasmas of LHD. Neutron yield measurement is essential for the LHD deuterium projects in terms of radiation safety, evaluation of fusion output, and study of energetic-particle confinement. To evaluate total neutron yield from LHD deuterium plasmas, wide dynamic range neutron flux monitor (NFM)[2] and neutron activation system (NAS) are employed in LHD.[3] The NFM on LHD consists of three ^{235}U fission chambers and three high-sensitivity thermal neutron detectors. The NFM plays a primary role in evaluating total neutron yield. Although NAS does not provide time evolution of neutron emission rate, it is absolutely insensitive to gamma-ray and is of great value to perform cross check of neutron yield evaluated by NFM.[4,5] The triton burnup study is one of the important physics subjects in the LHD deuterium project to demonstrate alpha particle confinement in the LHD-type magnetic field configuration. NAS also plays an important role in the triton burnup study through measurements of secondary 14.1 MeV neutron yield.

In the tokamaks such as TFTR[6], JET[7], ASDEX-U[8], and JT-60U[9], neutron activation techniques have been applied to measure neutron yield from deuterium plasmas. The activation response coefficients of NAS were evaluated from results of Monte Carlo neutron transport simulation code (MCNP)[10] in those devices. Limited points of in situ calibration experiments for NAS were performed in TFTR[11], JET[12], and FTU[13] by using neutron sources, but not by toroidal shape source. The machine structure of LHD is extremely complicated in comparison with tokamaks, and the activation response coefficients of NAS should be obtained from

3

experiment in addition to the simulation. LHD has enough space to install a railway, support structures, and a train loaded with the neutron source running along magnetic axis position inside the vacuum vessel to simulate a ring-shaped neutron source. In November, 2016, in situ absolute calibration of NFM and NAS were carried out in LHD by using an approximately 800 MBq ^{252}Cf neutron source. This in situ calibration of NAS was performed for the first time in the world on a fusion device.

In this paper, the introduction of NAS on LHD and calibration tools is described in Section II, the in situ calibration experiment is shown in Section III. The detection efficiencies of the high-purity germanium (HPGe) detector is discussed in Section IV. Activation response coefficients of NAS for 2.45 MeV neutron and secondary 14.1 MeV neutron from real deuterium plasma were evaluated from the activation response coefficient obtained in this calibration experiment. Those are discussed in Section V. Finally, the conclusions are given in Section VI.

II. EXPERIMENTAL SETUP
II-1. NEUTRON ACTIVATION SYSTEM ON LHD

NAS on LHD is a so-called rabbit system, consisting of activation foil, capsule, pneumatic control system, two irradiation ends, pneumatic tubes, air compressor, launching/collecting station, and two HPGe gamma-ray detectors as shown in Fig. 1(a). The system design of NAS is based on that used in JT-60U[9]. The activation foil is mounted into a capsule made of polyethylene. The capsule loaded with an activation foil is transferred through a pneumatic tube from the station to the irradiation end. There are two irradiation ends: one is at the 8-O horizontal port, which is located at the outboard side of the horizontally elongated

poloidal cross section of the plasma, and the other is located at the 2.5-L lower port, which is under the vertically elongated cross section of the plasma as shown in Fig. 1(b). Each irradiation end is made of stainless steel with coaxial structure. Outside of the port flange, the inner tube of the irradiation end is connected to a capsule transfer tube made of acrylonitrile-butadiene-styrene resin and the outer tube is connected to a vinyl chloride resin tube for compressed air supply and exhaust. The length of pneumatic tubes in the 8-O port line and the 2.5-L port line are 93 m and 80 m, respectively.

During the LHD experiment, the capsule will be transferred to the irradiation end before discharge initiation by receiving a trigger pulse before the discharge. After the discharge, the capsule will be transferred to the station for gamma-ray spectroscopy within the specified time. In the automatic control mode, this specified time can be set in the pneumatic control system by hand according to discharge duration. In the manual control mode, a capsule can be launched and transferred back any time whenever we want. Transferring time from the irradiation end to the station is about 20 s, which depends on the pressure of compressed air. Each tube has a manometer to monitor the air pressure.

The HPGe detector is essentially required to identify nuclides of our interest through gamma-ray spectroscopy with high energy resolution. The HPGe detector used in this work is manufactured by Canberra Industries, Inc. (Model: GX3018/CP5-PLUS-U). The detector has a very thin window made of carbon composite on the front surface, which reduces gamma-ray shielding effect of the window and extends the useful energy range down to 3 keV. Effective diameter and thickness of the germanium crystal of the HPGe detectors are 61.80 mm and 39.80 mm, respectively. The distance from the window to the surface of the HPGe detectors is 5.00 mm. Because the detector is in a lead shield having the thickness of 100 mm, the background

5

pulse counting rate due to external sources is low enough for our purpose. Output pulses from preamplifier are fed into the multichannel analyzer, the DSA-LX produced by Canberra Industries, Inc., based on advanced digital signal processing techniques, and data is analyzed on a personal computer.

The foil size is 10 mm in diameter and 1 mm in thickness. The indium foil is employed for the 2.45 MeV measurements utilizing ^{115}In(n, n')^{115m}In reaction, because the reaction has a threshold of 336 MeV, a half-life 4.486 h, and a rather large cross-section. For secondary 14.1 MeV neutron yield measurement, silicon and aluminum are used with ^{28}Si(n, p)^{28}Al, ^{27}Al(n, p)^{27}Mg, and ^{27}Al(n, α)^{24}Na reactions. Triton burnup ratio can be evaluated by the measurements of indium, silicon and aluminum. In this calibration experiment, a foil stack with 30 pieces of indium foils, as shown in Fig.1(c), is used to obtain the sufficient statistical error for much weaker neutron yield compared with that in real plasmas.

II-2. CALIBRATION NEUTRON SOURCE

To simulate toroidal plasma neutron source, the ring-shaped source must be created. Figure 2 (a) shows the source transport system by using a toy train rail with 36 mm rail width, the so-called O-gauge rail, and the train is loaded with a neutron source to circulate on the magnetic axis position at the major radius of 3.744 m inside the LHD vacuum chamber for generating a ring-shaped neutron source. The rail is fixed on the Bakelite plate which is installed on the maintenance stage made of aluminum frames as shown in Fig. 2(b).

An approximately 800 MBq ^{252}Cf neutron source by spontaneous fission was chosen for in situ calibration because the mean neutron energy of neutrons emitted from ^{252}Cf is approximately 2.1 MeV which is close to that of neutron produced by D-D reaction. The ^{252}Cf

neutron source emits 3.7 neutrons on average per every spontaneous fission event which is almost 3.1% of the decay. The half-life is approximately 2.646 years. The precise birth neutron emission rate was $(1.34\pm0.014) \times 10^8$ n/s at 12:00 GMT on 27 April 2015, which was calibrated at National Physics Laboratory, United Kingdom. Therefore, the birth neutron emission rate is $(8.91{\sim}8.95) \times 10^7$ n/s during this calibration experiment.

II-3. THE EFFICIENCIES OF THE HPGE DETECTOR

At the beginning, the detection efficiencies of the HPGe detector were calibrated by using the standard gamma-ray sources placed on the surface of the HPGe detector. The standard sources are the volumetric gamma-ray sources made by mixed powder gamma-ray sources of different types of nuclides in the U-8 container. The detection efficiencies obtained by using this source are shown in Fig. 3. In the in-situ calibration experiment, thirty pieces of activated foils ware placed on the surface of the HPGe detector. The geometry of the standard gamma-ray sources and the activated foil source are significantly different, therefore, the efficiencies of the HPGe detector for 336 keV (^{115m}In), 843 keV (^{27}Mg), 1368 keV (^{24}Na), and 1779 keV (^{28}Al) gamma-rays of the activated foils were evaluated with assist of the simulation calculation using Particle and Heavy Ion Transport code System (PHITS)[14] as shown in Fig. 3. Thirty pieces of foil stack were uniformly distributed on the surface of the HPGe detector in the model of the PHITS code. At first we calculated efficiencies of the 30 pieces of indium foil without the self-absorbed effect, which is the absorption of gamma rays by the foil material itself, where the foil density is assumed to be the same as the air density. Next we calculated detection efficiencies of 30 pieces of indium foil for 336 keV with the self-absorbed effect by using real density of the indium foil, where self-absorbed effect on the detection efficiency is clearly

observed. ~~In the results of the model with the self-absorbed effect, the self-absorbed effect of 30 pieces of indium foil for 336 keV is larger than the self-absorbed effect of 30 pieces of silicon foil and aluminum foil for high-energy gamma-rays.~~ Thus, we used the detection efficiency with the self-absorbed effect. In addition, the efficiencies of 1 piece of foil on the center of the surface of the HPGe detector with self-absorbed effect also were evaluated by the PHITS code for plasma experiments. In the 1 piece case model, the true sizes of HPGe detector and foil were also considered.

III. PRINCIPLE OF MEASUREMENT

The averaged neutron emission rate S_n [s^{-1}] can be calculated by the expression:

$$S_n = \frac{\lambda \cdot C}{N \cdot \alpha_\gamma \cdot \varepsilon \cdot (e^{-\lambda t_1} - e^{-\lambda t_2}) \cdot (1 - e^{-\lambda t_0}) \cdot \sum_E \sigma(E) \cdot \Phi(E)}.$$

In addition, total neutron yield can be obtained:

$$Y_n = S_n \cdot t_0.$$

Here, the activation response coefficients can be defined as reaction rate for unit source neutron and unit sample nuclei number. Thus the activation response coefficients of NAS can be expressed as follows:

$$\sum_E \sigma(E) \cdot \Phi(E) = \frac{\lambda \cdot C}{N \cdot S_n \cdot \alpha_\gamma \cdot \varepsilon \cdot (e^{-\lambda t_1} - e^{-\lambda t_2}) \cdot (1 - e^{-\lambda t_0})}.$$

In those expressions, $\sigma(E)$ is cross section of the reaction [b], $\Phi(E)$ is neutron spectrum in the irradiation end for unit source neutron [cm^{-2}·s^{-1}], E is neutron energy, $N = \alpha_{is} \cdot m \cdot N_A / M$ is the number of sample nuclei, α_{is} is the isotopic fraction of the sample nuclide, m is the mass of the sample [g], N_A is Avogadro's constant [mol^{-1}], M is the molar mass of the nuclide [g/mol], α_γ is gamma ray abundance, t_0 is the end of irradiation time [s], t_1 is start time of the gamma-

ray measurement from the start of the irradiation [s], t_2 is end time of the gamma-ray measurement from the start of the irradiation [s], λ is the decay constant of activated nuclide in the sample, C is gamma-ray count under the specific gamma-ray peak measured during from t_1 to t_2, and ε is the efficiency of the HPGe detector in the specific gamma-ray peak.[15]

IV. EXPERIMENTAL RESULTS

In the in situ calibration experiment, three capsules were irradiated over 15 hours at the 8-O port. Each capsule has 30 pieces of indium foil inside and the total mass of indium is approximately 18 g. Because 30 pieces of indium foil can not be transferred by the NAS pneumatic tube due to insufficient air pressure, the capsule was placed inside and removed by hand at the port. Immediately after the irradiation was finished, the capsule was removed for gamma-ray measurement. The irradiation times of capsule #1, capsule #2, and capsule #3 are 15.217 h, 15.583 h, and 46.283 h, respectively. Multiple measurements were performed to improve the statistical error and to eliminate the affect of the gamma-rays from ^{115}In(n, γ)^{116}In reactions. Each measurement time of the gamma-ray ranged from 3,000 s to 10,000 s in order to ensure that there are sufficient statistics of the photoelectric peak counts for the gamma-ray of interest. The integrated photoelectric peak pulse counts of 336 keV gamma-ray are evaluated by Gaussian fitting as shown in Fig. 4. Irradiated 30 pieces of indium foil were uniformly distributed on the surface of the HPGe detector and were measured simultaneously. The detection efficiencies of the HPGe detector for 30 pieces of indium foil measurement is evaluated by the PHITS code.

In Table 1, the activation response coefficients obtained by multiple gamma-ray measurements of each capsule are listed and those are plotted for each run number in Fig. 5.

The standard deviation of each counting is 12.85%. The error of the detection efficiencies of the HPGe detector from the PHITS calculation is 0.98%. Also, there is an error in irradiation time because it took approximately 2 minutes to place the capsule and to remove the capsule at the irradiation end. This error is considered to be 0.22% for total irradiation time of each capsule. The error of ^{252}Cf neutron source neutron emission rate is 1%. The total error of the calibration experiment is estimated to be approximately 12.92%. Thus the mean activation response coefficients of ^{115}In(n, n')^{115m}In reaction is evaluated to be $(9.40\pm1.21) \times 10^{-8}$.

V. DISCUSSION BASED ON MCNP SIMULATION

The neutron spectrum in the irradiation end $\Phi(E)$ normalized for unit source neutron is obtained from MCNP simulation. Activation response coefficients $\sum\sigma(E)\cdot\Phi(E)$ also can be obtained from MCNP simulation. Here MCNP6 code[10] and nuclear data library FENDL 3.0[16] are used for the $\Phi(E)$ calculation, and JENDL 99 Dosimetry file[17] is used for the reactivity calculation. The rotation time, about 40 s, of the calibration neutron source on the magnetic axis is sufficiently shorter than the half-life of ^{115m}In. Therefore, this source can be regarded as a toroidal ring-shaped source by averaging a long-time effect. Actually, the neutron source in the real plasma has poloidal distribution. The ^{252}Cf neutron source is a point source and is nearly isotropic in neutron emission. ~~This neutron source is not a volume neutron emission profile similar to an actual plasma source. Thus, this might lead to difference from $\Phi(E)$. To check the effect of difference in energy spectrum on the activation response coefficients, a three-dimensional neutron transport simulation by using the MCNP code is required.~~ The model for ^{252}Cf ring-shaped source is shown in Fig. 6(a), where detailed components are considered carefully, such as the irradiation end (enlarged part of Fig. 6(b)), the train, the railway, the

maintenance support, and the model of superconducting coils without liquid helium. In the ^{252}Cf

ring-shaped source case, source neutron energy has fission neutron spectrum represented by the

Watt formula[10] of *exp(-E/a) sinh (bE)$^{1/2}$*, where *a*=1.18 and *b*=1.03419. Also, foil stack of 30

pieces inside the capsule is modeled to estimate the self-shielding effect of the foil stack. The

activation response coefficients of ^{115}In(n, n')^{115m}In reaction for ^{252}Cf ring-shaped source case

was evaluated to be 8.80×10^{-8} (statistical error 4.23%) by MCNP calculation. It is in good

agreement with the result of the calibration experiment within 7% difference. Thus, the

correction factor of MCNP F_{cor} between experiment and MCNP can be obtained as follows:

$$F_{cor} = \frac{[\sum_E \sigma(E) \cdot \Phi(E)]_{exp.}}{[\sum_E \sigma(E) \cdot \Phi(E)]_{MCNP}}.$$

$[\sum \sigma(E) \cdot \Phi(E)]_{exp.}$ is activation response coefficient which is obtained from calibration

experiment or activation response coefficients for plasma experiment, and $[\sum \sigma(E) \cdot \Phi(E)]_{MCNP}$ is

activation response coefficient which was obtained from MCNP6. Thus, for this in situ

calibration, F_{cor} is evaluated to be 1.07, which indicates that the MCNP calculation taking

account of the self-shielding effect of the foil stack is sufficiently accurate.

In order to obtain the activation response coefficients for plasma source, difference

between the real plasma source and the ^{252}Cf ring-shaped source have been evaluated by MCNP.

In the model of real plasma, neutron source is a volumetrically mono-energetic neutron with a

neutron emission density profile which is the structure of five coaxial torus geometry as shown

in Fig. 6(b). The neutron emission probability of five coaxial torus regions is determined to fit

the typical neutron emission profile estimated in the LHD deuterium plasma. Also, only one

piece of activation foil is modeled to simulate the measurement at the real plasma experiment.

The model of superconducting coils has liquid helium. Other main structures of LHD are the

same. The neutron spectra normalized by unit source in the capsule without and with foil for the neutron from [252]Cf source, 2.45 MeV neutron, and 14.1 MeV neutron are shown in Fig.7 (a) and (b), respectively. In the incoming neutron spectra to the capsule shown in Fig. 7(a), there are significant differences in three spectra above 1 MeV because [252]Cf fission neutron spectrum has high-energy component, while neutron is mono-energetic in the plasma case. The low energy parts of spectra are almost the same. This means that scattered neutron from LHD models for [252]Cf ring-shaped source case and plasma case are almost the same. By comparing to Fig. 7(a) and Fig. 7(b), the large spectrum dip is found in the energy range of 1-5 eV for the capsule with 30 pieces of indium foil from the self-shielding effect of the foil stack for [252]Cf ring-shaped neutron source calculated by MCNP. Moreover, one piece of indium foil in the capsule was modeled for 2.45 MeV and 14 MeV plasma neutron source. Those would lead to the big different in low energy part of with foil case. Also, there are several differences in high-energy component from the self-shielding effect of the foil for neutron calculated by MCNP. The differences in the activation response coefficients are caused by the difference of incoming neutron spectrum to the capsule and the self-shielding effect of the foil stack for each reaction. We consider that the deviation of from unity is mainly due to the error of the modeling in the MCNP calculation. Therefore, F_{cor} obtained from in situ calibration experiment can be applicable not only for 2.45 MeV neutrons but also 14 MeV neutrons from the triton burnup process. The activation response coefficients for plasma case can be obtained as follow:

$$[\sum \sigma(E) \cdot \Phi(E)]_{plasma} = [\sum \sigma(E) \cdot \Phi(E)]_{\exp(^{252}Cf)} \times \frac{[\sum \sigma(E) \cdot \Phi(E)]_{MCNP(plasma)}}{[\sum \sigma(E) \cdot \Phi(E)]_{MCNP(^{252}Cf)}}$$

$$= F_{cor} \times [\sum \sigma(E) \cdot \Phi(E)]_{MCNP(plasma)}$$

As shown in Table 2, the activation response coefficient for 2.45 MeV neutron from the D-D plasma case and for secondary 14.1 MeV neutron are evaluated by using the MCNP calculation and F_{cor} to be 1.64×10^{-7} (statistical error 3.42%) of ^{115}In(n, n')^{115m}In reaction, 8.99×10^{-8} (statistical error 5.73%) of ^{28}Si(n, p)^{28}Al reaction, 2.52×10^{-8} (statistical error 5.64%) of ^{27}Al(n, p)^{27}Mg reaction, and 3.82×10^{-8} (statistical error 5.82%) of ^{27}Al(n, α)^{24}Na reaction, respectively.

VI. CONCLUSION

The activation response coefficients were obtained for the ^{252}Cf neutron source by using detection efficiency of the HPGe detector which was evaluated by the PHITS code. The activation response coefficients were in good agreement with the MCNP result. The activation response coefficients for 2.45 MeV neutron from D-D plasma and secondary 14.1 MeV neutron were evaluated from that for the ^{252}Cf neutron source with the assistance of the MCNP 6 calculation. This in situ calibration will be a good reference for future calibration experiments of fusion devices such as ITER.

REFERENCES

1 A. Iiyoshi, A. Komori, A. Ejiri, M. Emoto, H. Funaba, M. Goto, K. Ida, H. Idei, S. Inagaki, S. Kado, O. Kaneko, K. Kawahata, T. Kobuchi, S. Kubo, R. Kumazawa, S. Masuzaki, T. Minami, J. Miyazawa, T. Morisaki, S. Morita, S. Murakami, S. Muto, T. Mutoh, Y. Nagayama, Y. Nakamura, H. Nakanishi, K. Narihara, K. Nishimura, N. Noda, S. Ohdachi, N. Ohyabu, Y. Oka, M. Osakabe, T. Ozaki, B. J. Peterson, A. Sagara, S. Sakakibara, R. Sakamoto, H. Sasao, M. Sasao, K. Sato, M. Sato, T. Seki, T. Shimozuma, M. Shoji, H. Suzuki, Y. Takeiri, K. Tanaka, K. Toi, T. Tokuzawa, K. Tsumori, K. Tsuzuki, K.Y. Watanabe, T. Watari, H. Yamada, I. Yamada, S. Yamaguchi, M. Yokoyama, R. Akiyama, H. Chikaraishi, K. Haba, S. Hamaguchi, M. Iima, S.Imagawa, N. Inoue, K. Iwamoto, S. Kitagawa, J. Kodaira, Y. Kubota, R. Maekawa, T. Mito, T. Nagasaka, A. Nishimura, C. Takahashi, K. Takahata, Y. Takita, H. Tamura, T. Tsuzuki, S. Yamada, K. Yamauchi, N. Yanagi, H. Yonezu, Y. Hamada, K. Matsuoka, K.Murai, K. Ohkubo, I. Ohtake, M. Okamoto, S. Satoh, T. Satow, S. Sudo, S. Tanahashi, K. Yamazaki, M. Fujiwara, and O. Motojima, "Overview of the Large Helical Device project", Nucl. Fusion **39,** 1245 (1999).

2 M. Isobe, K. Ogawa, H. Miyake, H. Hayashi, T. Kobuchi, Y. Nakano, K. Watanabe, A. Uritani, T. Misawa, T. Nishitani, M. Tomitaka, T. Kumagai, Y. Mashiyama, D. Ito, S. Kono,

M. Yamauchi, and Y. Takeiri, "Wide dynamic range neutron flux monitor having fast time response for the Large Helical Device", Rev. Sci. Instrum, **85,** 11E114 (2014).

3 M. Isobe, H. Yamanishi, M. Osakabe, H. Miyake, H. Tomita, K. Watanabe, H. Iwai, Y. Nomura, N. Nishio, K. Ishii, J. H. Kaneko, J. Kawarabayashi, E. Takada, A. Uritani, M. Sasao, T. Iguchi, Y. Takeiri, and H. Yamada, "Fusion product diagnostics planned for Large Helical Device deuterium experiment", Rev. Sci. Instrum. **81**, 10D310 (2010).

4 L. C. Johnson, Cris W. Barnes, H. H. Duong, W. W. Heidbrink, D. L. Jassby, M. J. Loughlin, A. L. Roquemore, E. Ruskov, and J. D. Strachan, "Cross calibration of neutron detectors for deuterium-tritium operation in TFTR", Rev. Sci. Instrum, **66,** 894 (1995).

5 Cris W. Barnes, E. B. Nieschmidt, A. G. A. Huibers, L. P. Ku, R. W. Motley, and T. Saito, "Operation and cross calibration of the activation foil system on TFTR", Rev. Sci. Instrum, **61,** 3190 (1990).

6 C. W. Barnes, H.-S. Bosch, H. W. Hendel, A. G. A. Huibers, D. L. Jassby, R. W. Motley, E. B. Nieschmidt, T. Saito, J. D. Strachan, M. Bitter, R. V. Budny, K. W. Hill, D. K. Mansfield, D. C. Mccune, R. Nazikian, H. K. Park, A. T. Ramsey, S. D. Scott, G. Taylor, M. C. Zarnstorff "Triton burnup measurements and calculations on TFTR", Nucl. Fusion **38**, 597 (1998).

7 S. Conroy, O. N. Jarvis, G. Sadler, and G. B. Huxtable, "Time resolved measurements of triton burnup in JET plasmas", Nucl. Fusion **28**, 2127 (1988).

8 M. Hoek, H.-S. Bosch, and W. Ullrich, "Triton burnup measurements at ASDEX Upgrade by neutron foil activation", IPP-Report IPP-1/320 (1999).

9 M. Hoek, T. Nishitani, M. Carlsson, and T. Carlsson, "Triton burnup measurements by neutron activation at JT-60U", Nucl. Instrum. Meth. Phys. Res., A **368**, 804 (1996).

10 D. Pelowits (Ed.), MCNP6 Users Muanual, LA-CP-13-00634, Los Alamos National Laboratory (2013).

11 E. B. Nieschmidt, T. Saito, C. W. Barnes, H.-S. Bosch, and T. J. Murphy, "Calibration of the TFTR neutron activation system", Rev. Sci. Instrum, **59**, 1715 (1988).

12 D. B. Syme, S. Popovichev, S. Conroy, I. Lengar, L. Snoj, C. Sowden, L. Giacomellid, G. Hermona, P. Allan, P. Macheta, D. Plummer, J. Stephens, P. Batistoni, R. Prokopowicz, S. Jednorog, M. R. Abhangi, R. Makwanag, and JET EFDA Contributors, "Fusion yield measurements on JET and their calibration", Fus. Eng. Des. **89**, 2766 (2014).

13 M. Angelone, P. Batistoni, L. Bertalot, B. Esposito, M. Martone, M. Pillon, S. Podda, M. Rapisarda, and S. Roliet, "Experimental and numerical calibration of the neutron activation system on the FTU tokamak", Rev. Sci. Instrum, **61**, 3157 (1990).

14 T. Sato, K. Niita, N. Matsuda, S. Hashimoto, Y. Iwamoto, S. Noda, T. Ogawa, H. Iwase, H. Nakashima, T. Fukahori, K. Okumura, T. Kai, S. Chiba, T. Furuta, and L. Sihver, "Particle and Heavy Ion Transport code System, PHITS, version 2.52", J. Nucl. Sci. Technol. **50**, 913 (2013).

15 M. Hoek, T. Nishitani, Y. Ikeda, and A. Morioka, "Initial Results from Neutron Yield Measurements by Activation Technique at JT-60U", Japan Atomic Energy Research Institute, JAERI-M 94-002 (1994).

16 "Nuclear Data Libraries for Advanced Systems - Fusion Devices (FENDL 3.0)", Summary Report of the Third Research Coordination Meeting, IAEA, Vienna, Austria 6-9 December 2011.

17 K. Kobayashi, T. Iguchi, S. Iwasaki, T. Aoyama, S. Shimakawa, Y. Ikeda, N. Odano, K. Sakurai, K. Shibata. T. Nakagawa, and M. Nakazawa, "JENDL Dosimetry File 99 (JENDL/D-99)," Japan Atomic Energy Research Institute, JAERI 1344 (Jan. 2002).

Figure captions

Figure 1. (a) Overview of neutron activation system on LHD, (b) two irradiation ends of neutron activation system at two poloidal cross-sections of 8-O and 2.5-L ports, (c) the left photograph is of capsule, and the right photograph is of 30 pieces of indium foil on the surface of the HPGe detector.

Figure 2. (a) Horizontal layout diagram of in situ calibration experiment by using ^{252}Cf neutron source, (b) the photograph of railway inside the LHD vacuum vessel.

Figure 3. Detection efficiencies of the HPGe detector. "PHITS 1" represents calculation results of the case of 30 pieces of foil with self-shielding effect by the PHITS code. "PHITS 2" stands for the calculation results of the case of 30 pieces of foil without self-shielding effect. "PHITS 3" is the calculation results for the case of 1 piece of foil with self-shielding effect. Black points are detection efficiencies of the volume standard gamma-ray source for the HPGe detector.

Figure 4. (a)The gamma-ray spectrum, (b) the Gaussian fits of 336 keV gamma peak.

Figure 5. Activation response coefficients for ^{252}Cf ring-shaped neutron source.

Figure 6. (a) MCNP calculation model for ^{252}Cf source, (b) plasma model and enlarged irradiation end.

Figure 7. (a) The neutron spectra normalized by unit source in the capsule without the foil, (b) the neutron spectra normalized by unit source in the capsule with 30 pieces of indium foil in ^{252}Cf neutron case and 1 piece of foil in two plasma source cases.

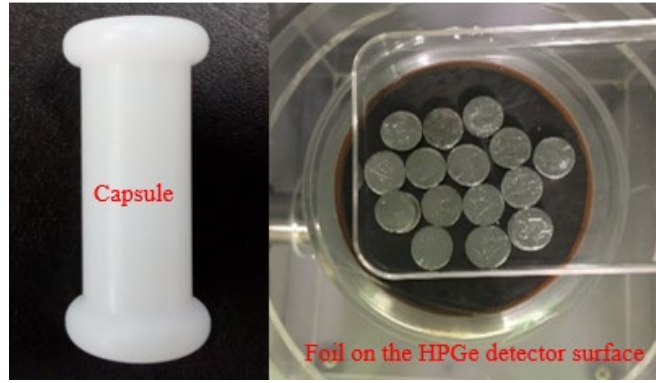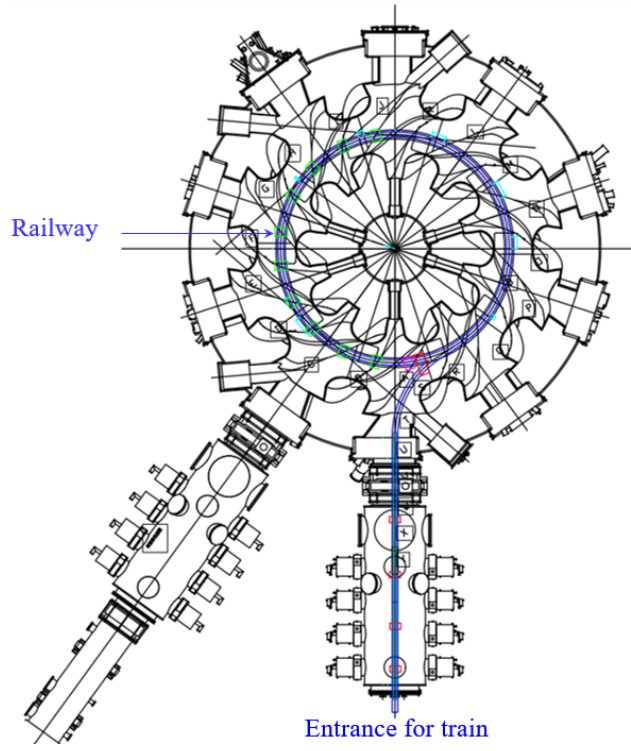Pneumatic tubes

Pneumatic control system
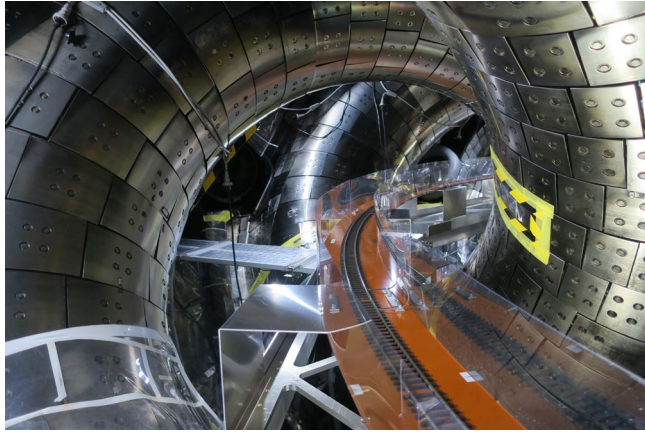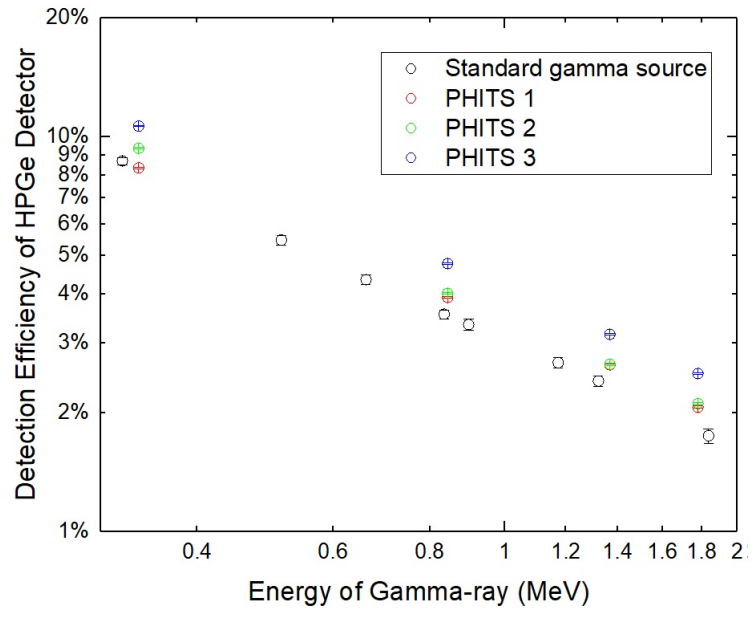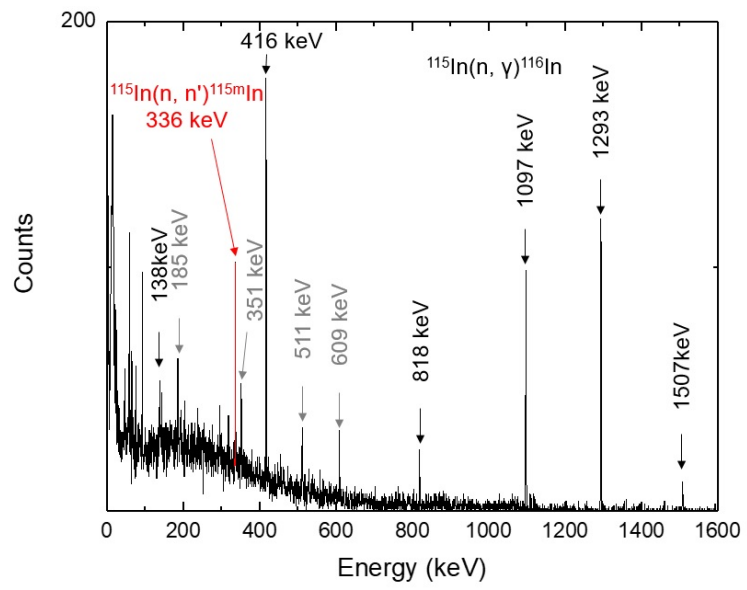
Station
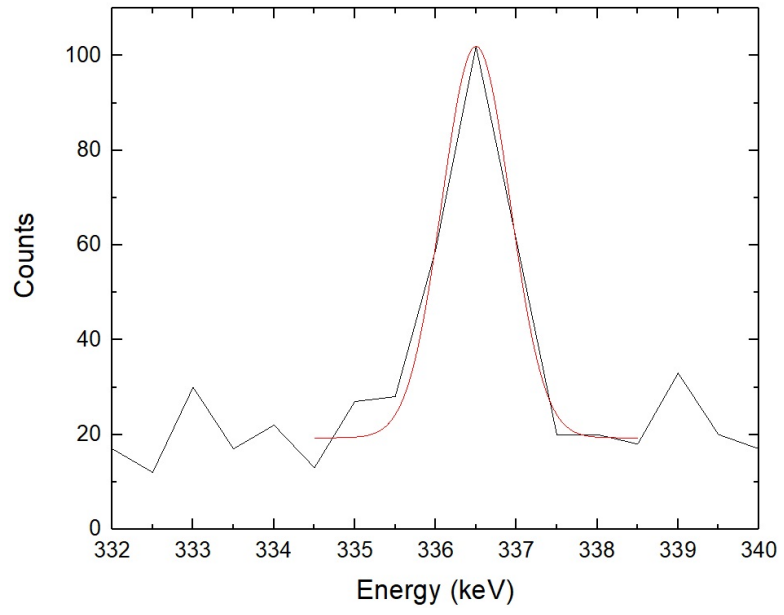
HPGe detector
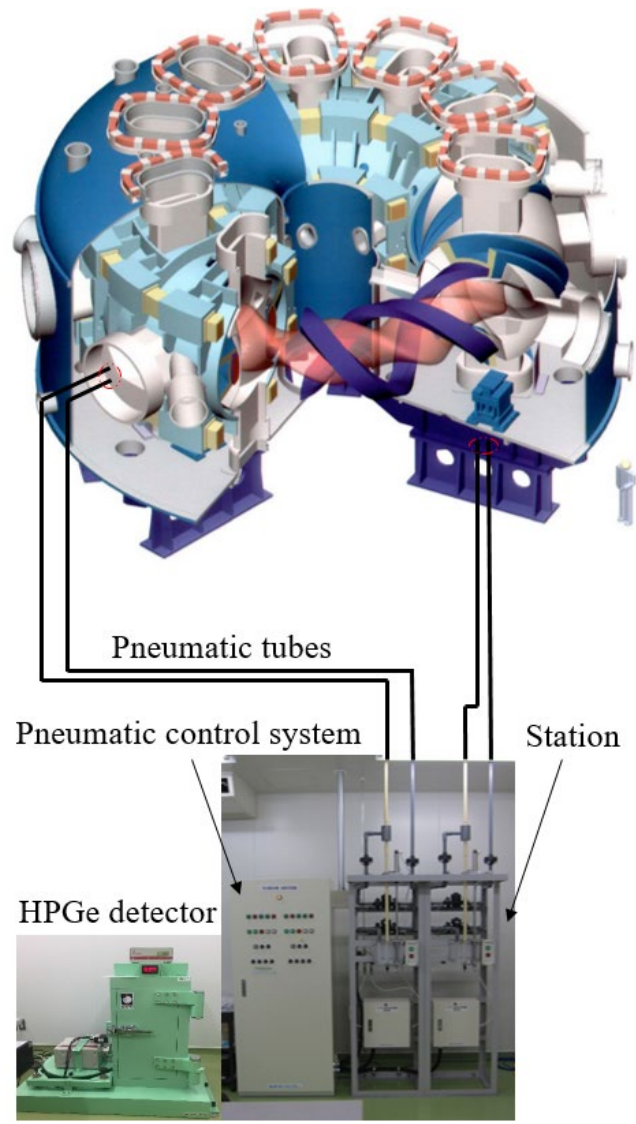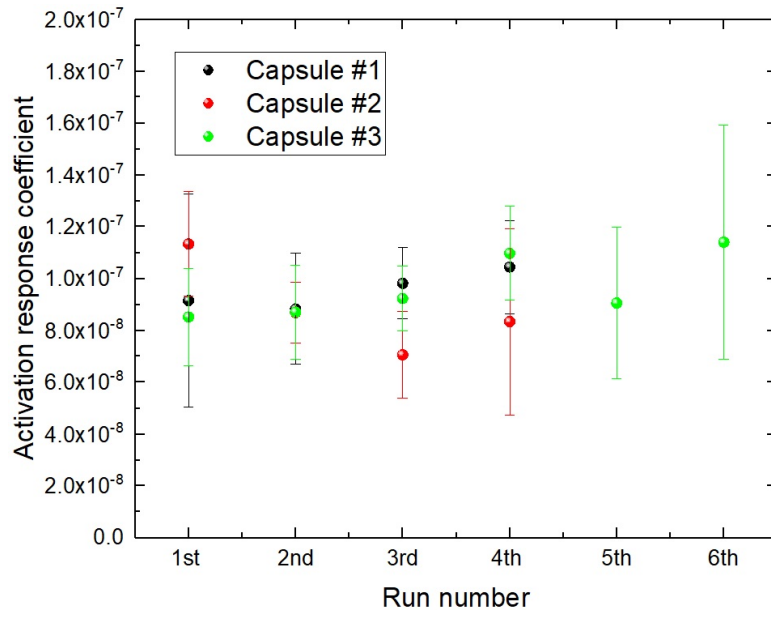
Fig. 1 (a)
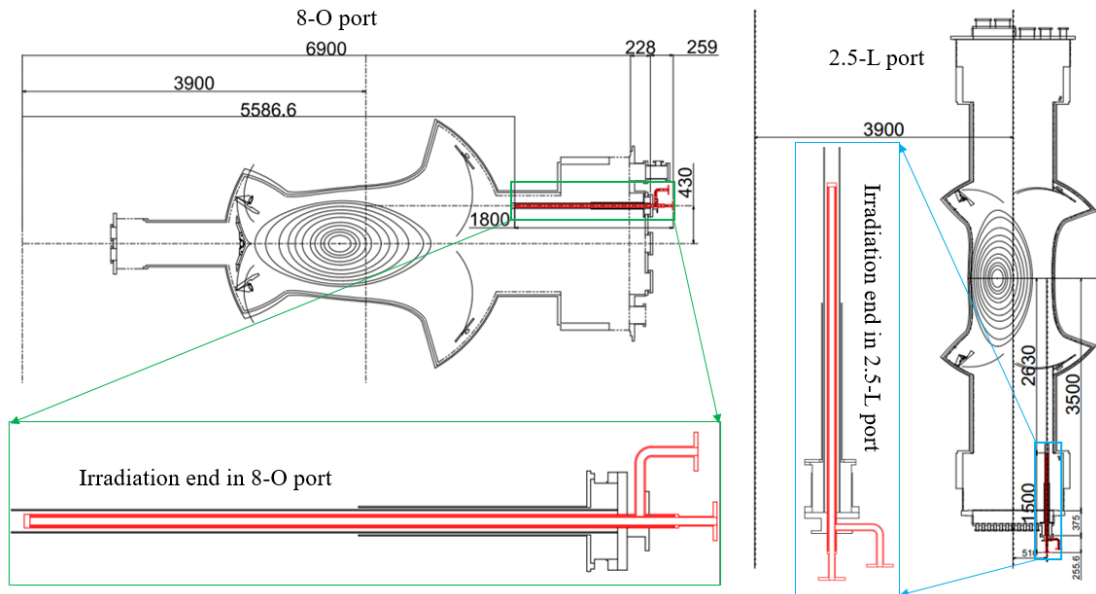
Fig. 1 (b)
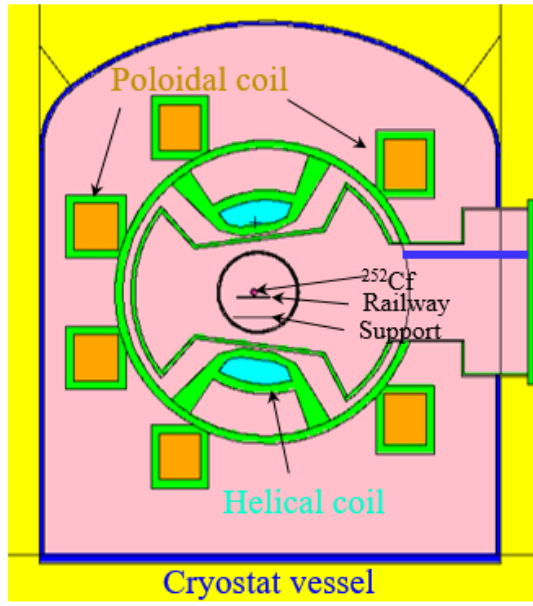
Fig.1 (c)

Fig. 2 (a)

Fig. 2 (b)

Fig. 3

Fig. 4(a)

Fig. 4(b)

Fig. 5

Fig. 6 (a)

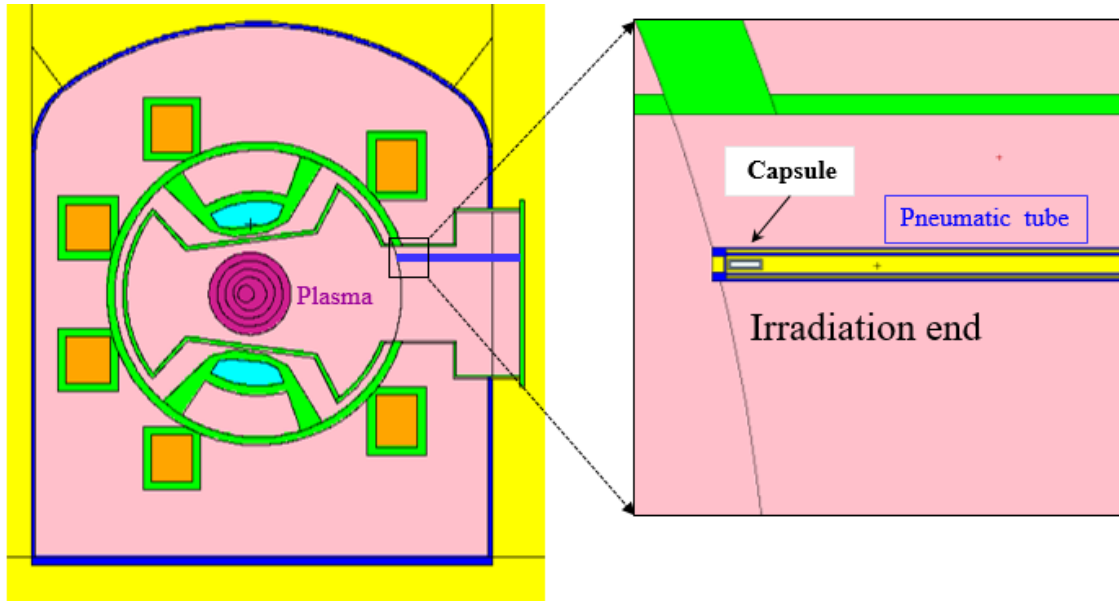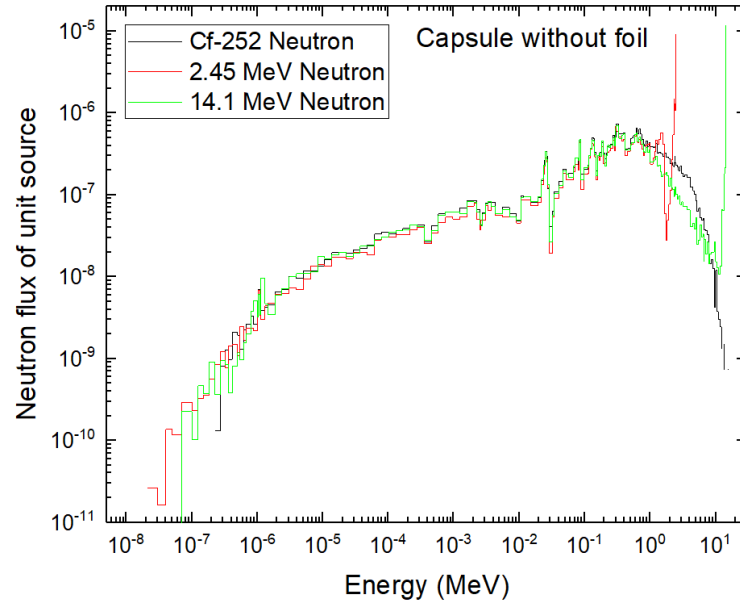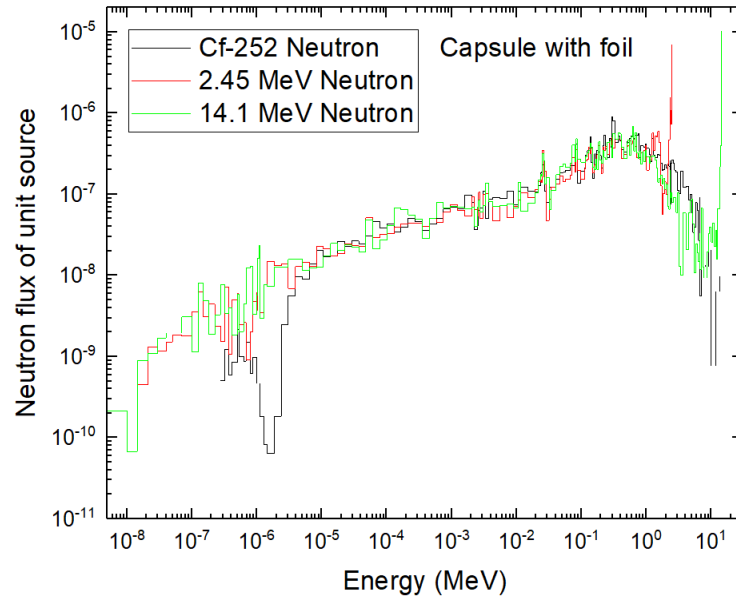Fig. 6 (b)

Fig. 7 (a)

Fig. 7 (b)

Table 1 Activation response coefficients (ARC) of ^{252}Cf ring-shaped source neutron source

	Capsule #1			Capsule #2			Capsule #3		
Mass	17.785 g			17.717 g			17.678 g		
Irradiation time	15.217 h			15.583 h			46.283 h		
Run number	Counting time	Counts	ARC	Counting time	Counts	ARC	Counting time	Counts	ARC
1st	3,000s	29.8	9.15×10^{-8}	3,000s	85.6	1.13×10^{-7}	3,000s	71.1	8.52×10^{-8}
2nd	3,000s	56	8.83×10^{-8}	10,000s	164.9	8.69×10^{-8}	3,000s	63.7	8.70×10^{-8}
3rd	10,000s	162	9.82×10^{-8}	10,000s	85	7.06×10^{-8}	10,000s	171.2	9.23×10^{-8}
4th	10,000s	111	1.04×10^{-7}	3,000s	22.375	8.34×10^{-8}	10,000s	121	1.10×10^{-7}
5th							10,000s	64.5	9.06×10^{-8}
6th							40,000s	115	1.14×10^{-7}

Table 2 Activation response coefficients for plasma case calculated by both the MCNP code and the correction factor F_{cor} for all reaction.

Reaction (neutron source)	Activation response coefficients	MCNP statistical error
^{115}In(n, n')^{115m}In (^{252}Cf neutron)	8.80×10^{-8}	4.23%
^{115}In(n, n')^{115m}In (2.45 MeV neutron)	1.64×10^{-7}	3.43%
^{28}Si(n, p)^{28}Al (14.1 MeV neutron)	8.99×10^{-8}	5.73%
^{27}Al(n, p)^{27}Mg (14.1 MeV neutron)	2.52×10^{-8}	5.64%
^{27}Al(n, α)^{24}Na (14.1 MeV neutron)	3.82×10^{-8}	5.82%